

Lightweight Cloud Masking Models for On-Board Inference in Hyperspectral Imaging

Mazen Ali, António Pereira, Fabio Gentile, Aser Cortines, Sam Mugel, Román Orús, Stelios P. Neophytides, Michalis Mavrovouniotis

Abstract—Cloud and cloud shadow masking is a crucial preprocessing step in hyperspectral satellite imaging, enabling the extraction of high-quality, analysis-ready data. This study evaluates various machine learning approaches, including gradient boosting methods such as XGBoost and LightGBM as well as convolutional neural networks (CNNs). All boosting and CNN models achieved accuracies exceeding 93%. Among the investigated models, the CNN with feature reduction emerged as the most efficient, offering a balance of high accuracy, low storage requirements, and rapid inference times on both CPUs and GPUs. Variations of this version, with only up to 597 trainable parameters, demonstrated the best trade-off in terms of deployment feasibility, accuracy, and computational efficiency. These results demonstrate the potential of lightweight artificial intelligence (AI) models for real-time hyperspectral image processing, supporting the development of on-board satellite AI systems for space-based applications.

Index Terms—Hyperspectral imaging, cloud masking, on-board inference, lightweight neural networks, satellite image processing, remote sensing, edge AI.

I. INTRODUCTION

SATELLITE remote sensing is essential for Earth observation, supporting downstream applications in environmental monitoring, disaster response, and land cover classification [1]. However, optical satellite imaging is often obstructed by clouds, necessitating cloud masking to retain only high-quality, unobstructed data for analysis [2].

Cloud masking methods generally fall into three categories:

- Physics-based methods use spectral thresholds to detect clouds efficiently but struggle with complex cloud structures [3, 4].
- Machine learning methods classify pixels based on spectral patterns but require labeled training data and adaptation for different sensors [5].
- Deep learning methods leverage CNNs to capture spatial and spectral patterns, achieving high accuracy but demanding significant computational resources [6, 7].

Hyperspectral Imaging (HSI) extends traditional remote sensing by capturing detailed spectral information across numerous bands, enabling precise surface and atmospheric characterization [8]. However, the high dimensionality of HSI data makes cloud and cloud shadow detection challenging, as

clouds exhibit diverse spectral signatures that can overlap with bright surfaces like snow, ice, and sand [9]. Traditionally, AI-based cloud masking has been performed on the ground due to its computational cost. However, advancements in onboard processing, including lightweight deep learning models and specialized hardware (e.g., FPGAs, VPUs), now enable AI-driven cloud segmentation directly on satellites.

As the era of CubeSats arrived with various on-board processing implementations, low energy consumption models have to be developed, due to satellites constraints [10]. Typically, a CubeSat of single, double or triple unit, operates with body mounted solar panels, generating limited power of about 5-8 watts [11]. At the same time, payloads such as integrated Field-Programmable Gate Arrays and Vision Processing Units, employed for the on-board processing tasks, in hyperspectral images, often require an energy consumption of about 12 W [12, 13].

This study focuses on leveraging novel techniques to improve model size reduction for higher utilization of on-board hardware and provision of analysis ready data directly from satellites. Our aim is to develop lightweight models for satellite on-board cloud masking in hyperspectral images. Specifically, 1) develop a high accuracy cloud detector using a public dataset, 2) reduce model sizes of CNNs, 3) test classical machine learning models as lightweight AI model alternatives for on-board processing and 4) integrate metadata-driven detection to optimize data utilization and reduce unnecessary down-linking.

The paper is structured as follows. Section III outlines the investigated models. Section IV presents performance evaluations. Section V discusses onboard processing feasibility. We provide a brief summary of the results in Section VI.

II. RELATED WORKS

The first ever on-board AI demonstrator was a cloud detector on Φ -Sat 1 satellite [14]. Upon the success of the Φ -Sat missions by the European Space Agency, the benefit from other various satellite on-board applications (e.g., vessel detection, image compression, crop health, wildfires, etc) has been identified [15, 16]. For example, on-board image compression can open new pathways for intelligent data processing as it reduces the needs for transmission bandwidth and storage [17]. In addition, solutions like CloudScout, an on-board cloud detector for hyperspectral imagery, can reduce the amount of data transmitted to satellite data acquisition stations by discarding cloudy pixels with a cloud detection accuracy of 92% [18]. An innovative space-grade Field-Programmable

M. Ali, A. Pereira, F. Gentile, A. Cortines, S. Mugel, R. Orús are with Multiverse Computing, San Sebastian, Spain. email: {mazen.ali, antonio.pereira, fabio.gentile, aser.cortines, sam.mugel, roman.orus}@multiversecomputing.com

S. Neophytides and M. Mavrovouniotis are with ERATOSTHENES Centre of Excellence and Cyprus University of Technology, Limassol, Cyprus. email: {stelios.neophytides, michalis.mavrovouniotis}@eratosthenes.org.cy

Gate Array (FPGA) was designed to host CloudScout pre-trained model with a 45% reduction in memory footprint with insignificant loss in accuracy, 24% reduction in energy consumption and a 2.4x speed-up at the cost of 1.8x higher power consumption in a benchmark comparison to the well-known Myriad 2 Vision Processing Unit [19].

An enhanced variation of the *function of mask (Fmask)* algorithm for segmentation of clouds on hyperspectral images derived by Gaofen mission showed a high accuracy of 95.51% [20]. Moreover, a dual-branch CNN for Gaofen-5 reached an F1-score of 94% [21]. A cloud detection model using hyperspectral layers related to atmospheric column water vapor from PRecurSore IperSpettrale della Missione Applicativa and Airborne Visible InfraRed Imaging Spectrometer-Next Generation satellite missions achieved an overall accuracy ranging from 97% to 100% on both sensors [22]. In addition, transfer learning techniques in fundamental NN architectures like ResNet50 and VGG16 showed that with a small dataset of 972 samples an accuracy over 90% can be reached for cloud detection in hyperspectral images [23]. Despite those studies showing a great capability in capturing the complex patterns of cloud detection, none of them investigated the potential of on-board processing.

More research studies like those for Hyper-Spectral Small Satellite for Ocean Observation [7, 24] are needed in the field of satellite on-board cloud detection with a special focus on the hardware constraints of processing units and the satellite itself. Thus, in this research study we are investigating new ways for reducing model size without significant accuracy trade-offs.

III. METHODS

Evaluating the task, type of data and available literature, we have selected the following approaches to investigate: XGBoost, LightGBM and CNNs. In the following, we give a brief description of each method.

A. XGBoost

Extreme Gradient Boosting (XGBoost [25]) is an ensemble learning method that has demonstrated strong performance across a wide range of applications [26], including cloud masking [5]. In ensemble learning, a robust predictive model is constructed by combining multiple weaker models.

In XGBoost, the weak learners are, by default, regression trees, also known as classification and regression trees (CARTs). The model iteratively enhances its predictions by adding new regression trees to the ensemble. XGBoost employs a level-wise tree growth strategy, meaning that at each growth step, the algorithm refines predictions by successively splitting each leaf node into two. As a result, the weak learners in the ensemble are balanced trees with $2^{\text{max_depth}}$ terminal nodes.

This approach is well-suited for handling large datasets with high-dimensional feature spaces, making it particularly relevant to our study. Additionally, the XGBoost software package [27] provides support for distributed learning and efficient large-scale data processing.

B. LightGBM

A potential limitation of XGBoost is that the number of leaves increases exponentially with tree depth, which can lead to computational inefficiencies. To mitigate this issue, particularly in scenarios requiring deeper trees, LightGBM offers an alternative approach.

Unlike XGBoost, which expands trees in a level-wise manner, LightGBM employs a leaf-wise growth strategy. It selectively expands only the leaf nodes where splitting a feature yields the greatest reduction in residual error. Consequently, the weak learners in LightGBM form unbalanced trees that can reach greater depths while maintaining a significantly lower number of leaves compared to XGBoost.

These optimizations, along with additional enhancements in the LightGBM library [28], enable more efficient training on large-scale datasets. However, a potential drawback of this approach is its susceptibility to overfitting, particularly when tree depth is excessively high.

C. Convolutional Neural Networks

Convolutional neural networks (CNNs) are among the most widely used architectures for image segmentation. The richness of spectral features in the dataset [29] allows for the use of relatively small CNN models while still achieving high predictive accuracy [7].

In [7], the authors obtained optimal results using a compact 1D CNN model. Here, “1D” refers to convolutions being applied exclusively along the spectral dimension for each pixel independently, without incorporating spatial context from neighboring pixels. As a baseline benchmark, we implement the same 1D CNN model in PyTorch, following the architecture described in [7]. However, we introduce a different data normalization technique – Z-score normalization – rather than the original method, which leads to an improvement in test accuracy.

To further reduce model size, we use Singularity™ to apply model compression based on the singular value decomposition of the convolutional layers in the CNN model [30].

Finally, we observed that on CPUs inference speed was primarily constrained by the high dimensionality of the input features. To address this, we used the principal component analysis tools (PCA) integrated within Multiverse Computing’s Singularity™ suite to reduce the feature space from 112 to 30, 18, 7 and 4 dimensions. We refer to these models as 1DJuLiNet, 1DJuLiNetSingularity, and 1DJuLiNetSingularityFx, with $x \in \{30, 18, 7, 4\}$, respectively.

IV. EXPERIMENTAL RESULTS

A. Experimental Setup

All experiments are performed on a g5.2xlarge AWS instance, equipped with an AMD EPYC 7R32 processor and a single NVIDIA A10G Tensor Core GPU with 24 GB of memory. The AMD EPYC 7R32 is a server-grade processor based on the Zen 2 architecture, featuring 8 physical cores, 16 threads (limited to 8 by the g5.2xlarge instance), and

TABLE I: Table representing the search space and optimal parameters for the XGBoost model.

Stage	Parameter Name	Type	Range	Optimal
1	max_depth	int	3 – 12	5
1	min_child_weight	int	1 – 10	3
2	subsample	float32	0.5 – 1.0	0.504
2	colsample_bytree	float32	0.5 – 1.0	0.779
3	learning_rate	float32	0.01 – 0.5	0.258
3	num_boost_round	int	50 – 1000	695

TABLE II: Table representing the search space and optimal parameters for the LightGBM model.

Stage	Parameter Name	Type	Range	Optimal
1	num_leaves	int	20 – 1000	28
1	min_data_in_leaf	int	20 – 2000	410
1	num_boost_round	int	50 – 200	140

a base clock speed of 3.2 GHz. The A10G GPU includes third-generation NVIDIA Tensor Cores optimized for machine learning workloads, delivering up to 250 TOPS of performance and 24 GB of dedicated memory. Full hardware specifications can be found on the AWS website.

A basic hyperparameter tuning was conducted for the boosting models while the hyperparameters for the CNN based models were kept identical to [7]. The reported experimental results correspond to the final optimized models only. For XGBoost, we performed a three-stage hyperparameter search using optuna (<https://optuna.org/> [31]) with limits and optimal parameters listed in Table I. While for LightGBM a single stage hyperparameter search was performed using the same tooling, see Table II.

B. Dataset Description

To develop and evaluate our cloud masking models, a labeled hyperspectral dataset of satellite imagery is required. Such data is scarce due to the high cost and complexity of hyperspectral imaging missions. The authors in [29] prepared one such suitable dataset, which is obtained from the HYPISO-1 mission and it is utilized in our experiments. The dataset provides labeled hyperspectral images captured by a 6U CubeSat carrying a hyperspectral imager.

The HYPISO-1 sensor system consists of a spectrometer with a 684-pixel slit, which sequentially scans 956 line frames to form a complete hyperspectral image, see [32, 33]. The resulting images have a spatial resolution of approximately 100 m \times 600 m, covering a wide area with high spectral fidelity. Each image comprises 120 spectral bands, spanning the 400 nm to 800 nm range with a spectral resolution of approximately 5 nm. This configuration enables detailed spectral analysis of surface and atmospheric conditions.

To ensure data consistency and accuracy, the raw sensor measurements undergo a two-step calibration process [29]. Spectral calibration is performed using a second-order polynomial fit, assigning precise wavelengths to each spectral band and storing them as metadata. Radiometric calibration then converts the raw digital number values into physical radiance values. Note that, for our study, only the radiance-calibrated

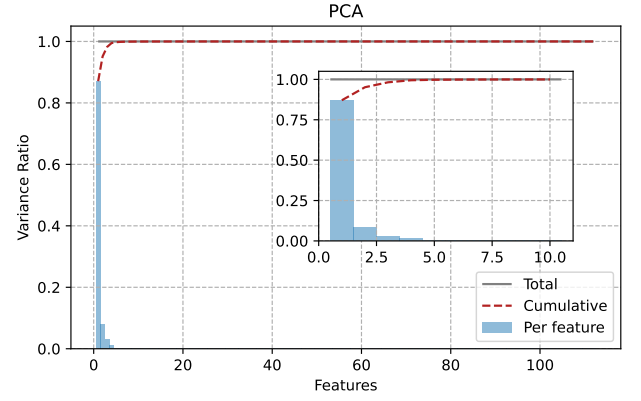


Fig. 1: Histogram of the principal components in decreasing order of amplitude and their cumulative distribution. The inset shows a zoom-in of the first 10 components.

data is utilized, as prior work has demonstrated its superior performance for hyperspectral analysis [29, 7].

The HYPISO-2 Sea-Land-Cloud-Labeled dataset consists of 38 labeled images, following the same train-validation-test split as the original study [7]. Specifically, 30 images are used for training, 3 images for validation, and 5 images for testing. In terms of pixels, the total is around 20, 2, and 3 million pixels for training, validation and testing, respectively, where each pixel consists of 120 spectral features. Note that 8 spectral bands are excluded due to known anomalies related to radiometric calibration or atmospheric light absorption as described in the original study. This leaves us with 112 spectral channels per pixel for model training, validation and testing. The dataset is openly accessible for download at the following website: https://ntnu-smallsat-lab.github.io/hypso1-sea_land_clouds_dataset/.

C. Model Training Comparison Experiment

While training time is not intended as a strict performance metric for on-board inference, it serves as an important indicator of computational demands and practical usability for preparing such models. All CNN models are trained for two epochs, following the approach in [7], as additional epochs did not yield improvements in validation accuracy.

Note that in the feature-reduced CNN models (1DJuLiNetSingularityFx), the non-trainable parameters correspond to the projection matrix in the initial layer, which projects the original feature space to a lower-dimensional vector space. To produce feature-reduced models, the most prominent components are plotted in decreasing order in Fig. 1. We observe that the first 7 main components account for over 99.9% of the total variance, while the largest 30 account for over 99.99% of the total variance. Therefore, four different feature-reduced CNN model variants are investigated – 1DJuLiNetSingularityFx, with $x \in \{30, 18, 7, 4\}$, i.e. 30, 18, 7 and 4 features, respectively.

Table III shows the results of the trained model sizes and an estimate of the training time. The results indicate that boosting models, i.e., XGBoost and LightGBM are the

TABLE III: Comparison of model size and training time for various cloud masking models. All models, except `LightGBM`, are trained on GPUs.

Model	Size (Parameter #)	Size (kB)	Training Time (min)
XGBoost	66 trees, 4104 nodes	264 (float64)	13
LightGBM	69 trees, 1932 nodes	228 (float64)	12
1DJuLiNetRetrained	4563	24 (float32)	42
1DJuLiNetSingularity	1419	12 (float32)	50
1DJuLiNetSingularityF30	597 trainable, 4554 total	20 (float32)	31
1DJuLiNetSingularityF18	525 trainable, 2541 total	13 (float32)	30
1DJuLiNetSingularityF07	63 trainable, 847 total	6 (float32)	28
1DJuLiNetSingularityF04	12 trainable, 487 total	5 (float32)	27

TABLE IV: Comparison of model accuracy metrics. All metrics given in % and they are computed on the test set for the cloud class only (cloud/no cloud).

Model	Accuracy	BOA	Precision	Recall	F1	Jaccard
XGBoost	93.32	90	92.7	78.32	84.91	73.78
LightGBM	93.33	90.04	89.33	78.59	83.62	71.85
1DJuLiNetRetrained	95.38	93.77	93.04	88.18	90.54	82.72
1DJuLiNetSingularity	93.47	90.91	93.8	82.27	87.67	78.04
1DJuLiNetSingularityF30	94.48	92.85	93.15	86.63	89.77	81.44
1DJuLiNetSingularityF18	91.60	90.20	81.59	84.21	82.88	70.77
1DJuLiNetSingularityF07	94.00	91.05	96.51	80.78	87.94	78.48
1DJuLiNetSingularityF04	92.93	88.11	94.47	71.39	81.33	68.53

fastest to train while maintaining relatively small parameter counts and model sizes. Among the CNN-based models, the compressed CNN (1DJuLiNetSingularity) together with 1DJuLiNetSingularityF07 and 1DJuLiNetSingularityF04 have the smallest overall parameter count and model size. It is worth mentioning that the two CNNs with feature reduction have the lowest number of trainable parameters, allowing them to achieve training speeds comparable to the booster models.

D. Accuracy Experiments

To identify appropriate evaluation metrics, it is important to align them with the practical goals of the application. The segmentation model is to be executed onboard the satellite to classify each pixel as cloud, land, or water, with the aim of estimating cloud coverage prior to image transmission. Based on this estimation, the system decides whether or not to download a given image. Since the presence of clouds is the main criterion for rejecting an image, performance on the cloud class is of primary importance. In particular, precision for the cloud class is critical, as false positives – pixels incorrectly labeled as cloud – can lead to discarding images that contain valuable land or water information. Additionally, the Jaccard index (IoU) provides a useful measure of the spatial accuracy of cloud segmentation, capturing the degree of overlap between predicted and true cloud regions. Finally, given the relatively mild class imbalance in this dataset, the difference between overall accuracy (BOA) and balanced overall accuracy remains small.

Table IV shows the classification results of the aforementioned metrics, the binary metrics being displayed for the cloud class only. As expected, the CNN model achieves the highest performance in nearly all the evaluation metrics, though the

other models also demonstrate strong performance. Fig. 2 presents the confusion matrices for each model, from which we can see that generally all the models are good predictors in all classes. The most populated class is “land” with about $\sim 1.71 \times 10^6$ samples, followed by “sea” with $\sim 1.25 \times 10^6$ samples, and finally “cloud” with about $\sim 0.46 \times 10^6$ samples. We observe that the 1DJuLiNetSingularityFx models tend to be better predictors for the “sea” class. While, the 1DJuLiNetSingularity, when compared to 1DJuLiNet model, mislabels significantly less true “land” for cloud, leaking more into the “sea” class.

Furthermore, Fig. 3 illustrates the pixel-level classification of the 5 samples from the test set. Each figure presents the actual image followed by the predicted, the ground-truth labeled and confidence probability. All models perform reasonably well on this test set, with a consistent misclassification of land pixels as sea pixels in the third image. Notably, the CNN model exhibits very high confidence across all images, which may indicate a suboptimal data split.

E. Inference Time Experiments

Table V summarizes inference times on a CPU and a GPU. For the CPU, times were consistent across different images. However, for the GPU the first image took much longer than subsequent images, and, hence, we provide the two time categories separately (i.e., GPU 1st Im. and GPU Rest). Note that, for `LightGBM`, we were unable to run inference on GPUs due to lacking software functionality.

From Table V, it can be observed that the CNN model is the slowest in terms of inference time whereas `XGBoost` is the fastest-performing model. On CPUs, both the CNN model and its compressed variants exhibit significantly slower inference times. On GPUs, the compressed CNN achieves a notable

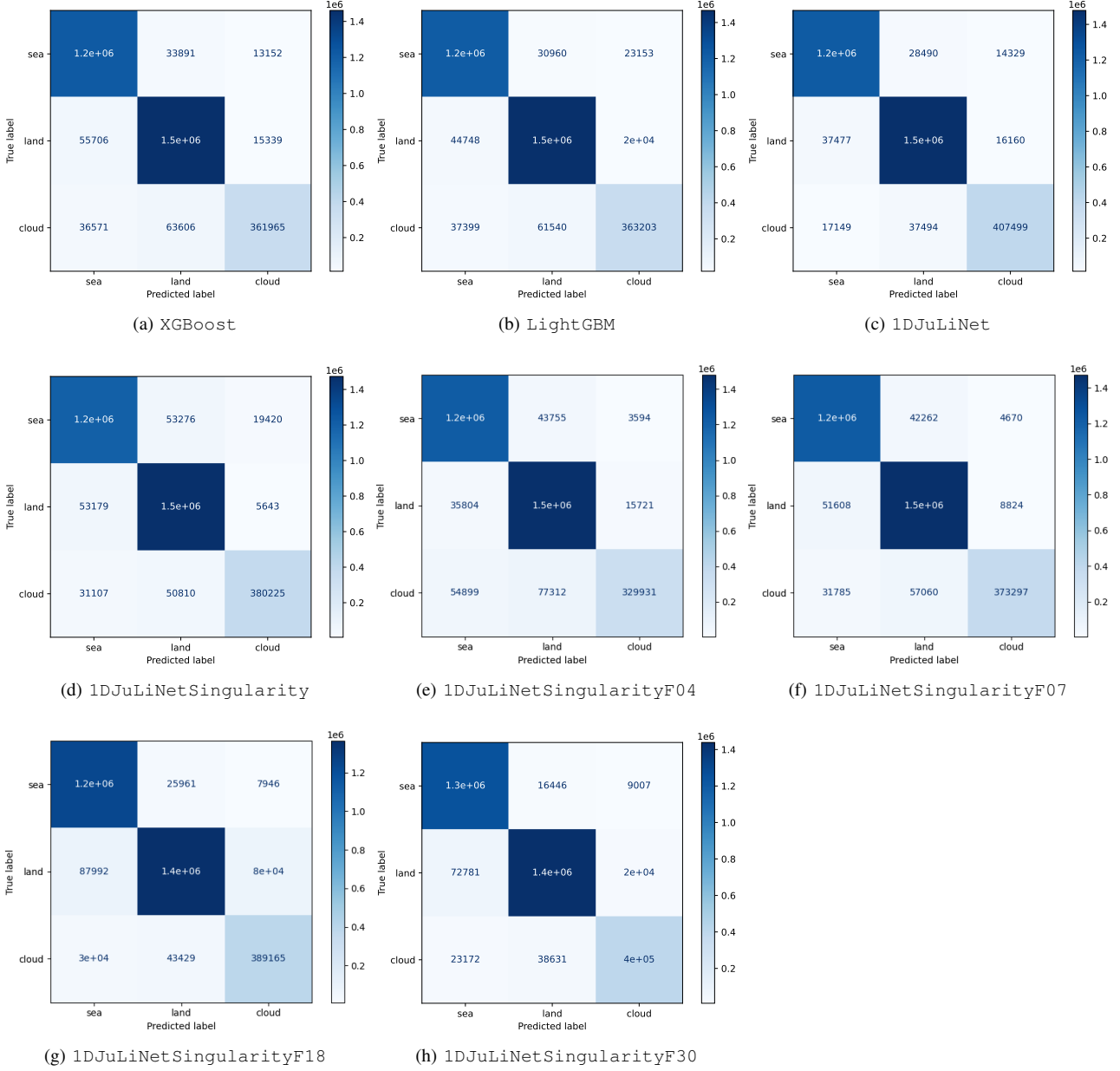


Fig. 2: Confusion matrices for different models.

speedup for the first image – processing it twice as fast as the uncompressed version – while inference times for subsequent images remain similar across all CNN variants. The CNN model with reduced features is by far the fastest among CNN-based models when running on CPUs.

V. DISCUSSION

An analytical two-step strategy is utilized to assess compatibility with components off the shelf hardware: an algorithm complexity analysis followed by a hardware feasibility mapping.

A. Complexity Analysis

The computational complexity of the model is assessed by estimating the floating point operations per second (FLOPS)

TABLE V: Comparison of model inference times. The times are given per image on the test image set.

Model	CPU	GPU 1st Im.	GPU Rest
XGBoost	240 ms	122 ms	50 ms
LightGBM	300 ms	–	–
1DJuLiNet	4.82 s	761 ms	1 ms
1DJuLiNetSingularity	5.62 s	316 ms	1 ms
1DJuLiNetSingularityF30	802 ms	710 ms	1 ms
1DJuLiNetSingularityF18	421 ms	254 ms	1 ms
1DJuLiNetSingularityF07	278 ms	215 ms	1 ms
1DJuLiNetSingularityF04	218 ms	215 ms	1 ms

required at each processing stage. This analysis enables a detailed characterization of the model's computational load and facilitates the screening of hardware candidates capable

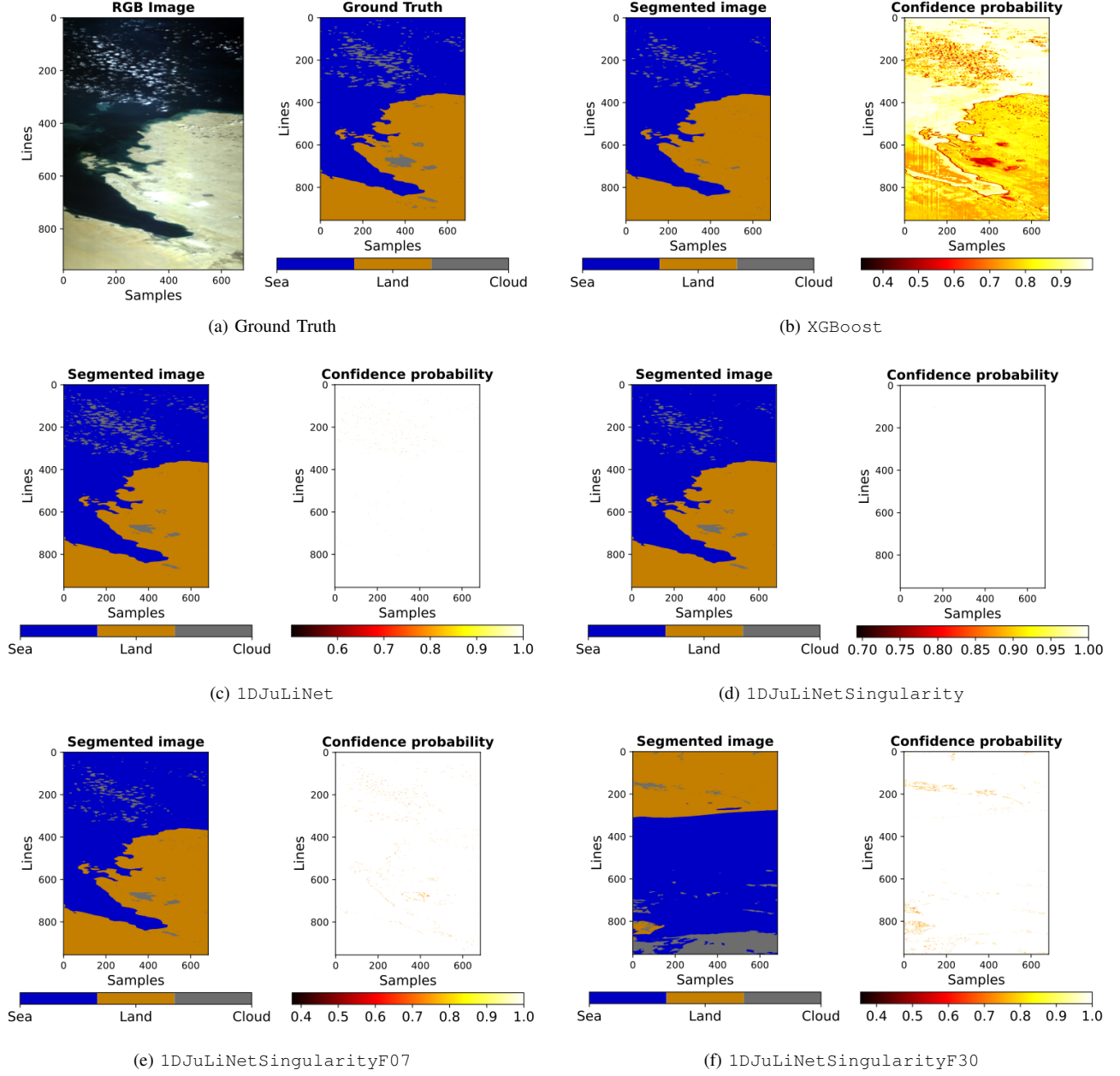


Fig. 3: Comparison of (a) Ground truth, (b) XGBoost, (c) 1DJuLiNet, (d) 1DJuLiNetSingularity, (e) 1DJuLiNetSingularityF07, and (f) 1DJuLiNetSingularityF30 on the sample representing Qatar.

of supporting the required workload. In Table VI, the outcome of this evaluation is reported.

From Table VI, it is evident how the compression and feature-reduction layers notably reduce the complexity of the model without significantly affecting performance (see Table IV for a performance summary).

Besides the evaluation of the computational operations and comparison, the CPU inference time can be used as a uniform metric to compare different models. To select the most appropriate algorithm, we display a diagram in Fig. 8, showing different metrics for each model and the associated inference time. This diagram showcases that computational resources can be reduced by an order of magnitude without significantly

decreasing prediction quality.

B. Feasibility Mapping

The resource requirements of the model – specifically processing throughput, memory usage, and power consumption – are critical factors in assessing its suitability for deployment on edge devices, particularly for onboard satellite applications.

In their work, Justo et al. [7] evaluated the feasibility of deploying their model on the hardware platform of the HYPSON-1 satellite. This platform features a Zynq-7030 System-on-Chip (SoC), which integrates a dual-core ARM Cortex-A9 CPU and a Kintex-7 FPGA for onboard data processing. The system provides 32 KB of L1 data cache for memory access, enabling

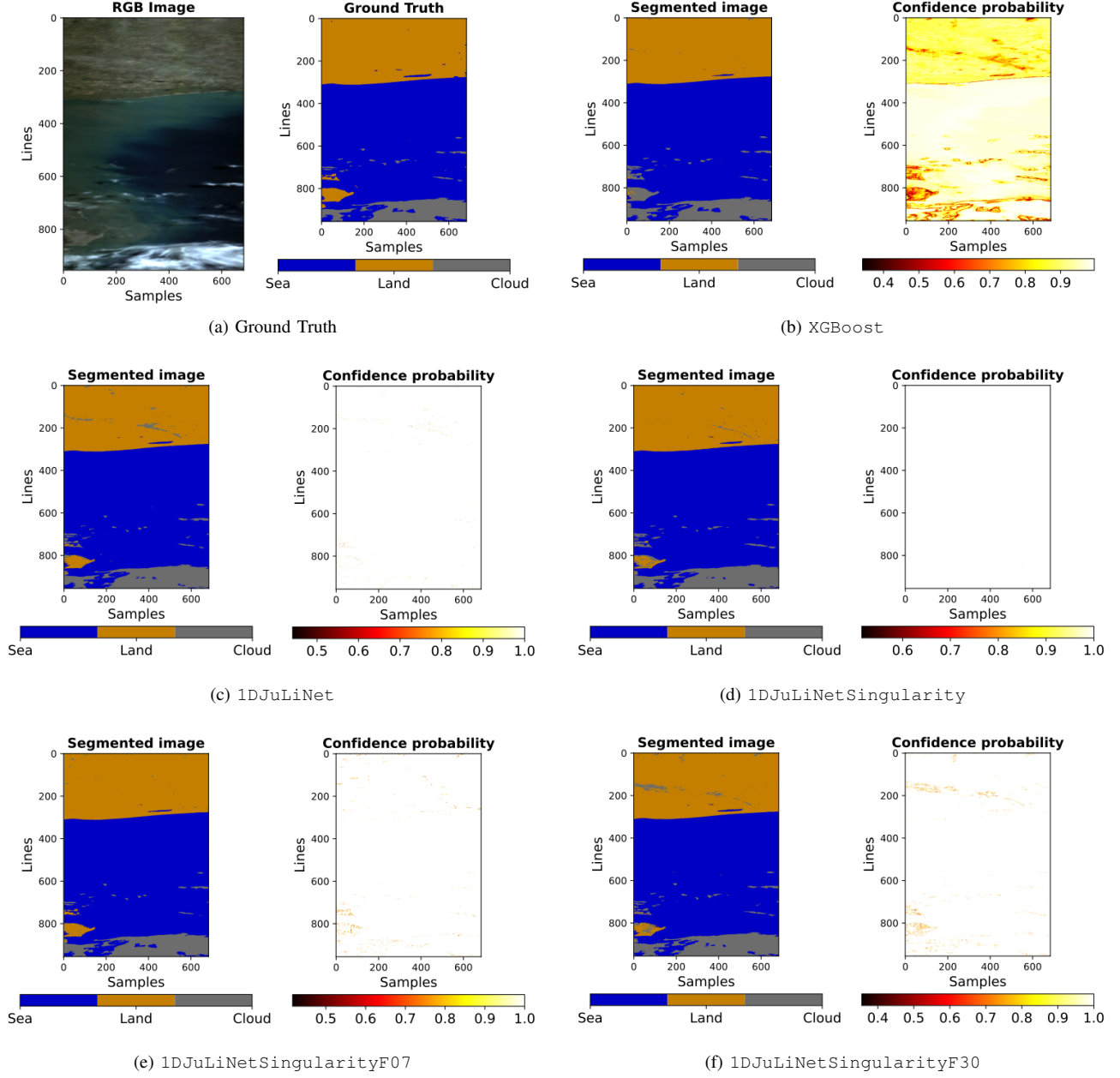


Fig. 4: Comparison of (a) Ground truth, (b) XGBoost, (c) 1DJuLiNet, (d) 1DJuLiNetSingularity, (e) 1DJuLiNetSingularityF07, and (f) 1DJuLiNetSingularityF30 on the sample representing Argentina.

storage of up to 8K model parameters when encoded in 4-byte format. They demonstrated that the 1DJuLiNet model, comprising only of 4563 parameters, is compatible with this hardware. Subsequently, in a later study, Justo et al. [24] reported a successful onboard deployment of 1DJuLiNet on the HYPSON-1 satellite.

In contrast to 1DJuLiNet, we introduce several alternative models that exhibit lower parameter counts (see Table III), comparable or improved performance (while the original model achieved an estimated accuracy of 93% in [7], our retraining attained over 95%, with most of the compressed and boosting models surpassing 93% accuracy – refer to Table IV), and significantly reduced computational demands.

Among these, 1DJuLiNetSingularity model achieves a 65% reduction in FLOPS with very similar prediction scores with half of the memory footprint (only 12 kB instead of 24 kB) and about one third of the original trainable parameters (1419 parameters, instead of 4563). Recall that 1DJuLiNetSingularity is obtained through a tensor network based compression [34], where convolutional layers are replaced by tensorized layers using the Multiverse Computing’s Singularity™ (Deep Learning) suite.

Furthermore, the model 1DJuLiNetSingularityF30 reduces the input space dimension through principal component analysis achieving 87.6% FLOPS reduction, while the XGBoost model requires as few as 66 FLOPS and 330

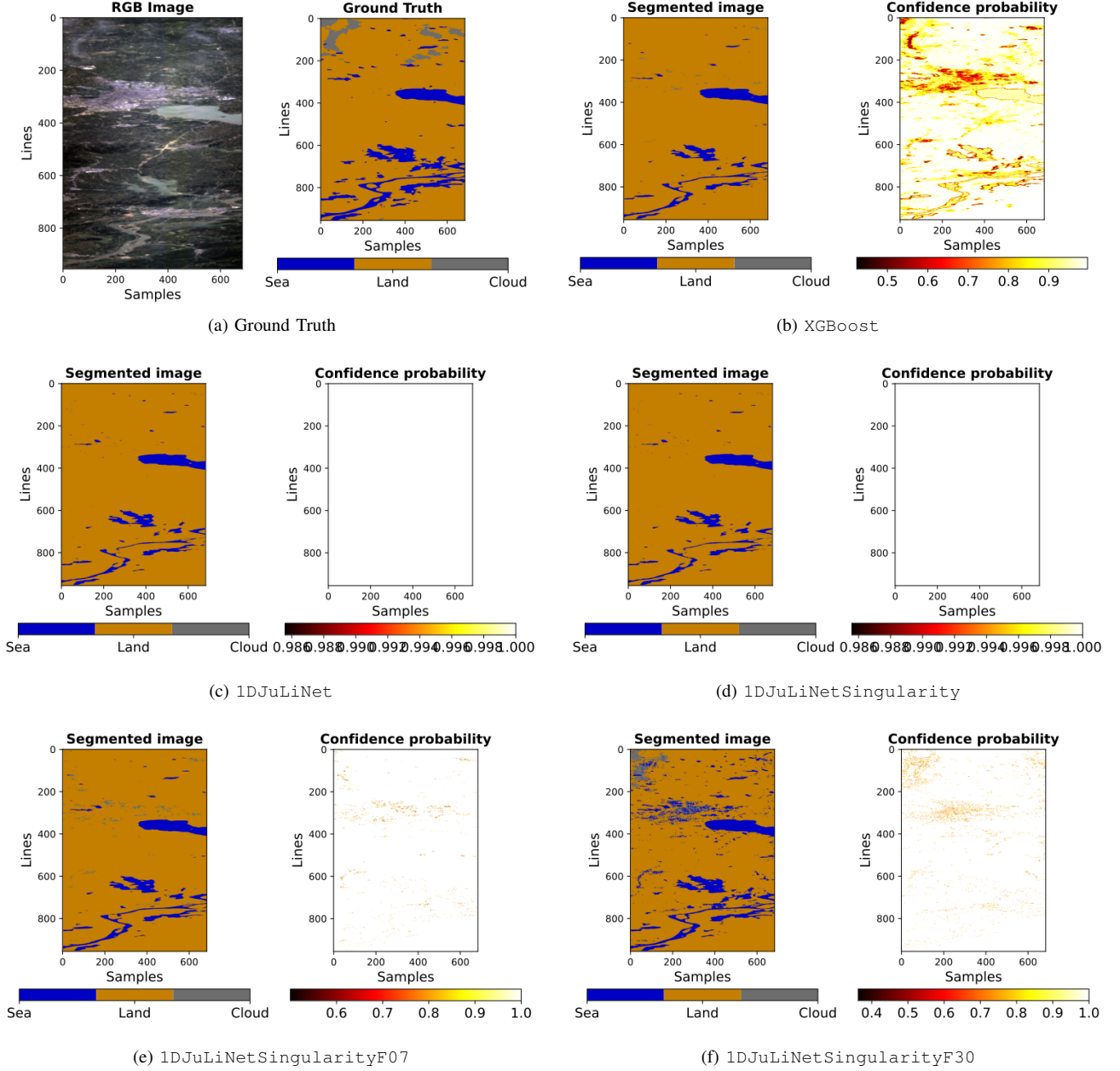


Fig. 5: Comparison of (a) Ground truth, (b) XGBoost, (c) 1DJuLiNet, (d) 1DJuLiNetSingularity, (e) 1DJuLiNetSingularityF07, and (f) 1DJuLiNetSingularityF30 on the sample representing China.

floating-point comparisons (see Table VI). These results do not only confirm the feasibility of deploying these models onboard, but also demonstrate improvements in inference latency (see Table V and Figure 8), and indicate potential improvements in energy efficiency. These findings support the practical viability of deploying lightweight CNN models, particularly feature-reduced variants, in budget-constrained satellite missions.

VI. CONCLUSIONS

In this study, multiple machine learning approaches are evaluated for on-board cloud masking in hyperspectral satellite imagery. The investigated models

include gradient boosting methods (XGBoost and LightGBM), CNNs (1DJuLiNet), compressed CNNs (1DJuLiNetSingularity), and CNNs using feature reduction techniques (1DJuLiNetSingularityFx, where $x = 4, 7, 18, 30$).

Our experimental results demonstrate that all boosting and CNN-based models performed well, achieving over 93% classification accuracy, with CNN models exceeding 95% accuracy. Additionally, all models have proved to be lightweight, with trainable parameter counts ranging from 12 to 4500 and storage requirements between 5kB and 265kB. The 1DJuLiNetSingularity model was among the smallest in storage at 12kB, with the absolute smallest being the

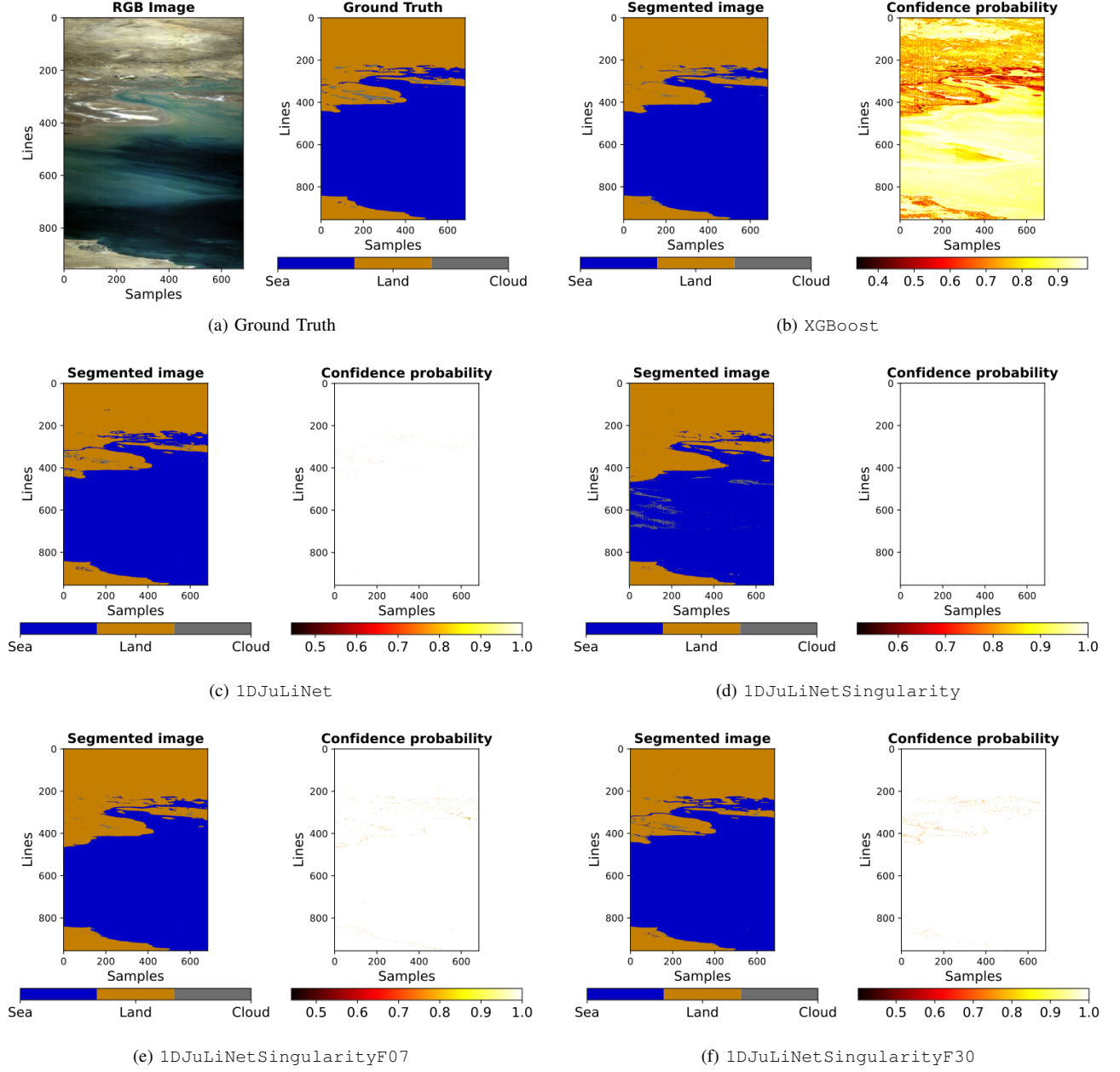


Fig. 6: Comparison of (a) Ground truth, (b) XGBoost, (c) 1DJuLiNet, (d) 1DJuLiNetSingularity, (e) 1DJuLiNetSingularityF07, and (f) 1DJuLiNetSingularityF30 on the sample representing Iran.

1DJuLiNetSingularityF07 model, counting only 12 training parameters and requiring just 5 kB of storage.

Inference speed varied by architecture and hardware:

- On GPUs, all models ran efficiently, with CNNs achieving around 1 ms per image and XGBoost requiring up to 50 ms per image.
- XGBoost presents the smallest computational footprint (with only 66 FLOPS and 300 floating-point comparisons) with fast inference of 240 ms per image, while the most accurate CNNs were significantly slower at 4 s to 5 s per image. However, the 1DJuLiNetSingularityF30 model significantly improved CPU performance, reducing inference time to

800 ms per image, making it a viable candidate for low-power deployment scenarios.

Training efficiency also varied:

- Boosting models were the fastest to train, completing training in just ~ 12 min on both CPUs and GPUs.
- CNNs required 27 min to 50 min for two epochs, while the 1DJuLiNetSingularityF30 improved training efficiency, completing in 16 min.

Considering accuracy, model size, training efficiency, and inference speed, the model 1DJuLiNetSingularityF30 emerged as the best overall choice. It maintained a high accuracy ($> 94\%$), had one of the smallest storage footprints (20KB), required only 597 trainable parameters, and signifi-

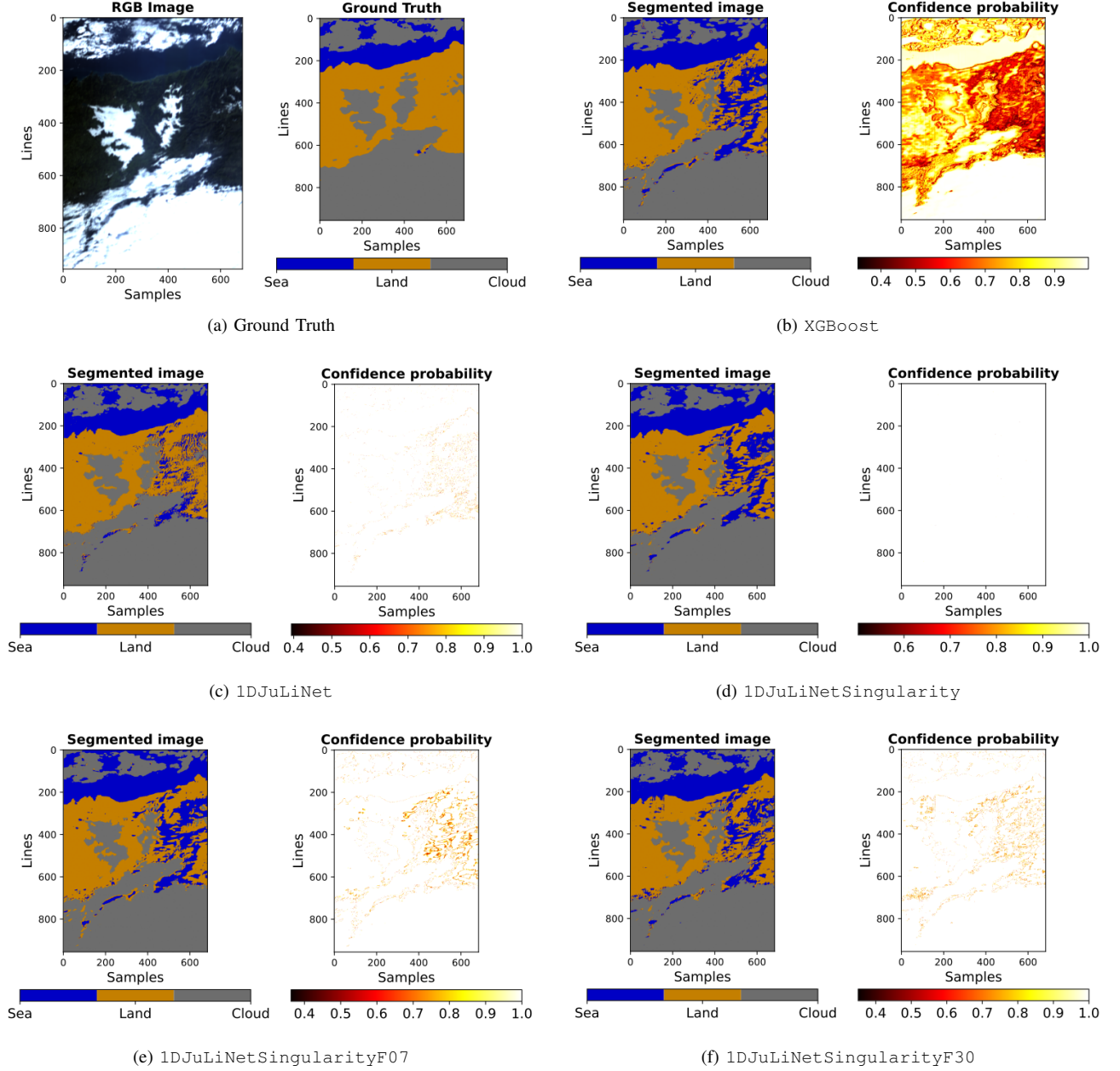


Fig. 7: Comparison of (a) Ground truth, (b) XGBoost, (c) 1DJuLiNet, (d) 1DJuLiNetSingularity, (e) 1DJuLiNetSingularityF07, and (f) 1DJuLiNetSingularityF30 on the sample representing Spain.

cantly improved inference speed on CPUs (800 ms per image) while remaining fast on GPUs.

This work shows that lightweight AI models can be a practical solution for real-time cloud and cloud shadow masking on hyperspectral imagery. The evaluated models performed consistently well, with high accuracy and low computational cost, even under constraints typical of satellite hardware. That said, the study focused on one dataset (HYPSO-1), which, while well-suited for benchmarking, does not cover the full range of environments or sensor configurations satellites might encounter. Moreover, although hardware compatibility was carefully assessed through computational complexity measurements, the models were not deployed on real satellite systems

in this phase. These aspects do not detract from the results but rather point to natural next steps to confirm the robustness of these models in a wider range of conditions.

ACKNOWLEDGMENT

This work was supported by the “ENFIELD: European Lighthouse to Manifest Trustworthy and Green AI” initiative under the 1st Innovation Scheme Open Call, specifically addressing the vertical VS.1 – “AI Satellite On-Board Processing Model for Cloud and Cloud Shadow Masking on Hyperspectral Images with a Metadata Perspective”.

TABLE VI: Comparison of model complexities. This table clearly highlights the decrease of computational complexity of various models w.r.t. 1DJuLiNet. Compressing the model leads to an about 63% reduction in the number operations, while feature-reduction offers a gradual trade-off between performance and efficiency. It is noteworthy that boosting models do not make use of floating point operations per se, besides weighted averaging, but rather work on Floating point Comparisons (COMP).

Model	kFLOPS / pixel	COMP / pixel
XGBoost	~ 0.066	~ 330
LightGBM	~ 0.069	(214–754)
1DJuLiNet	124.42	–
1DJuLiNetSingularity	45.99	–
1DJuLiNetSingularityF30	15.49	–
1DJuLiNetSingularityF18	6.17	–
1DJuLiNetSingularityF07	1.79	–
1DJuLiNetSingularityF04	1.06	–

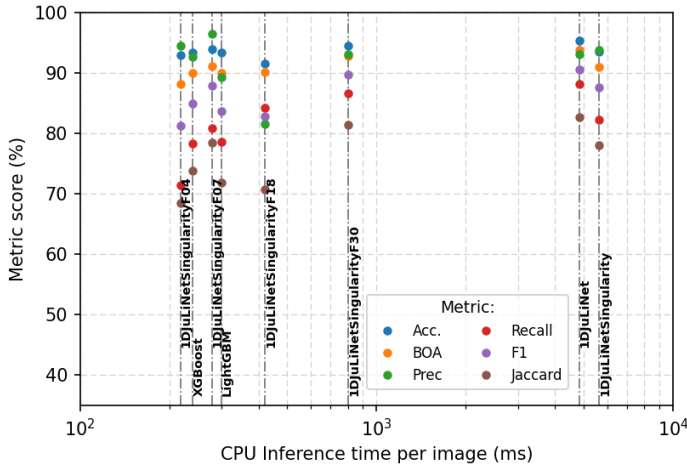


Fig. 8: Diagram of prediction quality of studied models compared with their CPU’s inference time per image in ms. Inference time, and therefore model complexity can be reduced by over one order of magnitude at the cost of a small decrease in prediction quality.

REFERENCES

- [1] Devis Tuia et al. “Artificial Intelligence to Advance Earth Observation: A review of models, recent trends, and pathways forward”. In: *IEEE Geoscience and Remote Sensing Magazine* (2024), pp. 2–25. DOI: [10.1109/MGRS.2024.3425961](https://doi.org/10.1109/MGRS.2024.3425961).
- [2] Anna Anzalone, Antonio Pagliaro, and Antonio Tutton. “An Introduction to Machine and Deep Learning Methods for Cloud Masking Applications”. In: *Applied Sciences* 14.7 (2024). ISSN: 2076-3417. DOI: [10.3390/app14072887](https://doi.org/10.3390/app14072887). URL: <https://www.mdpi.com/2076-3417/14/7/2887>.
- [3] Magdalena Main-Knorn et al. “Sen2Cor for Sentinel-2”. In: *Image and Signal Processing for Remote Sensing XXIII*. Ed. by Lorenzo Bruzzone. Vol. 10427. International Society for Optics and Photonics. SPIE, 2017, p. 1042704. DOI: [10.1117/12.2278218](https://doi.org/10.1117/12.2278218). URL: <https://doi.org/10.1117/12.2278218>.
- [4] Shi Qiu, Zhe Zhu, and Binbin He. “Fmask 4.0: Improved cloud and cloud shadow detection in Landsats 4–8 and Sentinel-2 imagery”. In: *Remote Sensing of Environment* 231 (2019), p. 111205. ISSN: 0034-4257. DOI: <https://doi.org/10.1016/j.rse.2019.05.024>. URL: <https://www.sciencedirect.com/science/article/pii/S0034425719302172>.
- [5] Anze Zupanc. *Improving Cloud Detection with Machine Learning*. Accessed: 2025-04-01. 2017. URL: <https://medium.com/sentinel-hub/improving-cloud-detection-with-machine-learning-c09dc5d7cf13>.
- [6] Nicholas Wright et al. “CloudS2Mask: A novel deep learning approach for improved cloud and cloud shadow masking in Sentinel-2 imagery”. In: *Remote Sensing of Environment* 306 (2024), p. 114122. ISSN: 0034-4257. DOI: <https://doi.org/10.1016/j.rse.2024.114122>. URL: <https://www.sciencedirect.com/science/article/pii/S0034425724001330>.
- [7] Jon Alvarez Justo et al. *Semantic Segmentation in Satellite Hyperspectral Imagery by Deep Learning*. 2024. arXiv: [2310.16210](https://arxiv.org/abs/2310.16210) [cs.CV]. URL: <https://arxiv.org/abs/2310.16210>.
- [8] Pedram Ghamisi et al. “Advances in Hyperspectral Image and Signal Processing: A Comprehensive Overview of the State of the Art”. In: *IEEE Geoscience and Remote Sensing Magazine* 5.4 (2017), pp. 37–78. DOI: [10.1109/MGRS.2017.2762087](https://doi.org/10.1109/MGRS.2017.2762087).
- [9] Han Zhai et al. “Cloud/shadow detection based on spectral indices for multi/hyperspectral optical remote sensing imagery”. In: *ISPRS Journal of Photogrammetry and Remote Sensing* 144 (2018), pp. 235–253. ISSN: 0924-2716. DOI: <https://doi.org/10.1016/j.isprsjprs.2018.07.006>. URL: <https://www.sciencedirect.com/science/article/pii/S0924271618301989>.
- [10] Usama Shakoor, Mohanad Alayedi, and Ebrahim E. Elsayed. “Comprehensive analysis of Cubesat electrical power systems for efficient energy management”. In: *Discover Energy* 5.1 (Apr. 2025), p. 9. ISSN: 2730-7719. DOI: [10.1007/s43937-025-00069-5](https://doi.org/10.1007/s43937-025-00069-5). URL: <https://doi.org/10.1007/s43937-025-00069-5>.
- [11] Gulama-Garip Alisher E. Ibrayev et al. “Reducing Energy Consumption in CubeSat Missions: The Integrated Antenna Approach”. In: *Engineered Science* 33 (2025), p. 1315. DOI: [10.30919/es1315](https://doi.org/10.30919/es1315).
- [12] Scott Sterling Arnold, Ryan Nuzzaci, and Ann Gordon-Ross. “Energy budgeting for CubeSats with an integrated FPGA”. In: *2012 IEEE Aerospace Conference*. 2012, pp. 1–14. DOI: [10.1109/AERO.2012.6187240](https://doi.org/10.1109/AERO.2012.6187240).
- [13] Oleksandr Liubimov and Ihor Turkin. “Optimizing the CubeSat On-Board Computer Power Consumption Under Hard Real-Time Constraints”. In: *Integrated Computer Technologies in Mechanical Engineering - 2023*. Ed. by Mykola Nechyporuk, Volodymyr Pavlikov, and Dmytro Krytskyi. Cham: Springer Nature Switzerland, 2024, pp. 404–414. ISBN: 978-3-031-60549-9.

- [14] Gianluca Giuffrida et al. “The Phi-Sat-1 Mission: The First On-Board Deep Neural Network Demonstrator for Satellite Earth Observation”. In: *IEEE Transactions on Geoscience and Remote Sensing* 60 (2022), pp. 1–14. DOI: [10.1109/TGRS.2021.3125567](https://doi.org/10.1109/TGRS.2021.3125567).
- [15] Alessandro Marin et al. “Phi-Sat-2: Onboard AI Apps for Earth Observation”. en. In: (2021).
- [16] Nicolas Longépé et al. “Simulation of Multispectral and Hyperspectral EO Products for Onboard Machine Learning Application”. In: *IEEE Journal of Selected Topics in Applied Earth Observations and Remote Sensing* 17 (2024), pp. 17651–17665. DOI: [10.1109/JSTARS.2024.3434437](https://doi.org/10.1109/JSTARS.2024.3434437).
- [17] Giorgia Guerrisi, Fabio Del Frate, and Giovanni Schiavon. “Artificial Intelligence Based On-Board Image Compression for the Phi-Sat-2 Mission”. In: *IEEE Journal of Selected Topics in Applied Earth Observations and Remote Sensing* 16 (2023), pp. 8063–8075. DOI: [10.1109/JSTARS.2023.3296485](https://doi.org/10.1109/JSTARS.2023.3296485).
- [18] Gianluca Giuffrida et al. “CloudScout: A Deep Neural Network for On-Board Cloud Detection on Hyperspectral Images”. In: *Remote Sensing* 12.14 (2020). ISSN: 2072-4292. DOI: [10.3390/rs12142205](https://doi.org/10.3390/rs12142205). URL: <https://www.mdpi.com/2072-4292/12/14/2205>.
- [19] Emilio Rapuano et al. “An FPGA-Based Hardware Accelerator for CNNs Inference on Board Satellites: Benchmarking with Myriad 2-Based Solution for the CloudScout Case Study”. In: *Remote Sensing* 13.8 (2021). ISSN: 2072-4292. DOI: [10.3390/rs13081518](https://doi.org/10.3390/rs13081518). URL: <https://www.mdpi.com/2072-4292/13/8/1518>.
- [20] Xiaomeng Yang et al. “An Improved Fmask Method for Cloud Detection in GF-6 WFV Based on Spectral-Contextual Information”. In: *Remote Sensing* 13.23 (2021). ISSN: 2072-4292. DOI: [10.3390/rs13234936](https://doi.org/10.3390/rs13234936). URL: <https://www.mdpi.com/2072-4292/13/23/4936>.
- [21] Junchuan Yu et al. “An Effective Cloud Detection Method for Gaofen-5 Images via Deep Learning”. In: *Remote Sensing* 12.13 (2020). ISSN: 2072-4292. DOI: [10.3390/rs12132106](https://doi.org/10.3390/rs12132106). URL: <https://www.mdpi.com/2072-4292/12/13/2106>.
- [22] Alexandre Alakian. “Cloud Detection in Hyperspectral Images with Atmospheric Column Water Vapor: Application to PRISMA and AVIRIS-NG Images”. In: *IEEE Transactions on Geoscience and Remote Sensing* 62 (2024), pp. 1–24. DOI: [10.1109/TGRS.2024.3369401](https://doi.org/10.1109/TGRS.2024.3369401).
- [23] Wang Jian et al. “Transfer-learning-based cloud detection for Zhuhai-1 satellite hyperspectral imagery”. In: *Frontiers in Environmental Science* Volume 10 - 2022 (2022). ISSN: 2296-665X. DOI: [10.3389/fenvs.2022.1039249](https://doi.org/10.3389/fenvs.2022.1039249). URL: <https://www.frontiersin.org/journals/environmental-science/articles/10.3389/fenvs.2022.1039249>.
- [24] Jon Alvarez Justo et al. “Hyperspectral Image Segmentation for Optimal Satellite Operations: In-Orbit Deployment of 1D-CNN”. In: *Remote Sensing* 17.4 (2025). ISSN: 2072-4292. DOI: [10.3390/rs17040642](https://doi.org/10.3390/rs17040642). URL: <https://www.mdpi.com/2072-4292/17/4/642>.
- [25] Tianqi Chen and Carlos Guestrin. “XGBoost: A Scalable Tree Boosting System”. In: *Proceedings of the 22nd ACM SIGKDD International Conference on Knowledge Discovery and Data Mining*. KDD ’16. Association for Computing Machinery, 2016, 785–794. ISBN: 9781450342322. DOI: [10.1145/2939672.2939785](https://doi.org/10.1145/2939672.2939785). URL: <https://doi.org/10.1145/2939672.2939785>.
- [26] *Machine Learning Challenge Winning Solutions*. Accessed: 2025-04-01. URL: <https://github.com/dmlc/xgboost/tree/master/demo#machine-learning-challenge-winning-solutions>.
- [27] *XGBoost*. Accessed: 2025-04-01. URL: <https://xgboost.readthedocs.io/>.
- [28] *LightGBM*. Accessed: 2025-04-01. URL: <https://lightgbm.readthedocs.io/>.
- [29] Jon A Justo et al. “An Open Hyperspectral Dataset with Sea-Land-Cloud Ground-Truth from the Hypso-1 Satellite”. In: *2023 13th Workshop on Hyperspectral Imaging and Signal Processing: Evolution in Remote Sensing (WHISPERS)*. IEEE. 2023, pp. 1–5.
- [30] Brenda Praggastis et al. *The SVD of Convolutional Weights: A CNN Interpretability Framework*. 2022. arXiv: [2208.06894](https://arxiv.org/abs/2208.06894) [cs.CV]. URL: <https://arxiv.org/abs/2208.06894>.
- [31] Takuya Akiba et al. *Optuna: A Next-generation Hyperparameter Optimization Framework*. 2019. arXiv: [1907.10902](https://arxiv.org/abs/1907.10902) [cs.LG]. URL: <https://arxiv.org/abs/1907.10902>.
- [32] Sivert Bakken et al. “HYPISO-1 CubeSat: First Images and In-Orbit Characterization”. In: *Remote Sensing* 15.3 (2023). ISSN: 2072-4292. DOI: [10.3390/rs15030755](https://doi.org/10.3390/rs15030755). URL: <https://www.mdpi.com/2072-4292/15/3/755>.
- [33] Elizabeth Prentice et al. “Design of a hyperspectral imager using COTS optics for small satellite applications”. In: June 2021. DOI: [10.1117/12.2599937](https://doi.org/10.1117/12.2599937).
- [34] Román Orús. “A practical introduction to tensor networks: Matrix product states and projected entangled pair states”. In: *Annals of Physics* 349 (2014), pp. 117–158. ISSN: 0003-4916. DOI: <https://doi.org/10.1016/j.aop.2014.06.013>. URL: <https://www.sciencedirect.com/science/article/pii/S0003491614001596>.